Scaling in quasifree hadron-nucleus charge-exchange reactions

R. J. Peterson*

Department of Physics, University of Colorado Boulder, Boulder, Colorado 80309-0390, USA

(Received 21 June 2019; published 6 November 2019)

The formalism developed for hadron quasifree scattering to infer relativistic single-nucleon responses is extended to data for hadronic charge exchange for a wide range of beams and nuclear samples. Scaling tests of the first, second, and third kinds are applied to the results.

DOI: 10.1103/PhysRevC.100.054602

I. INTRODUCTION

It is possible to investigate the nature and behavior of nucleons within complex nuclei directly by scattering from them individually under appropriate kinematic conditions [1]. Meeting these requirements on beam momentum, beam energy, and momentum transfer will allow quasifree incoherent scattering from individual nucleons, based upon free beam-nucleon cross sections. Many experimental studies of such quasifree electron scattering data have been pursued [2,3], with extensive theoretical efforts to model these results [4–8], often by comparing data through anticipated scaling relations derived from the quasifree mechanism.

Quasifree scattering of hadrons from bound nucleons offers even broader studies, albeit with complications due to the strong interactions. Scaling tests of hadron quasifree scattering without charge exchange (NCX) have recently been presented, with demonstrations of scaling versus several variables taken to demonstrate that the scattering was indeed quasifree, and thus that the inferred responses do indeed represent the nature and interactions of bound nucleons [9]. Here, these scaling tests are applied to the same responses extracted from data for hadron scattering with single charge exchange (SCX) of the beam hadron.

Charge exchange inclusive quasifree scattering, either $(\pi, \pi^0 \mathrm{x})$ (with both beam pion charge states) or $(p,n\mathrm{x})$, must be driven by isovector ($\Delta T = 1$) interactions with a single bound nucleon, much as found for quasifree transverse electron scattering (here labeled as EET). Examples of transverse electron scattering responses will be shown for comparison. Hadron quasifree scattering without charge exchange (NCX) is driven largely by isoscalar interactions, and NCX responses have been presented in Ref. [9].

Neutrino interactions with nuclei are of recent interest, with the detected particles also resulting from charge changing reactions on nuclei. Theories of these interactions have been tested by comparison to electron scattering data [10], but hadron beam charge exchange data can provide other tests, such as those simulated by large cascade calculations [11].

In this work a large collection of hadron SCX spectra at beam energies appropriate to meet the quasifree conditions [1] will be transformed to relativistic responses $\Phi(\psi)$ by the same methods as used for hadronic NCX quasifree data, as presented in the Appendix of Ref. [9]. These responses will be subjected to three tests of scaling, that is independence from a single variable, for many three-momentum transfers q (or scattering angles), target masses A, beam energies and beam species (electron, π^+,π^-, proton). A special case of exclusive (one-and-only-one neutral pion) will also be considered, using the data of Ref. [12]. These SCX scaling responses will be presented much as for their NCX companions [9]. These relativistic responses to hadron SCX will be compared to the same responses taken from the transverse electron scattering results for several nuclei and momentum transfers from the data of Ref. [13].

Scaling of the first kind has been defined [4,14,15] as the same responses being found for a given nuclear sample A and a given beam species across a range of three-momentum transfers q. For hadrons, these analyses will also use a given hadron beam energy, since the couplings among hadrons will depend upon these beam energies. Scaling of the second kind has been defined as observing the same responses for a given beam at the same momentum transfer for all nuclear samples of mass A [14,15]. Simultaneous scaling of both the first and second kinds has been called "superscaling" [4]. Scaling of the third kind would be noted if responses at a given momentum transfer and for a given nucleus are found to be the same for all beams, electrons and hadrons. If all three kinds of scaling are found across some regions of the variables, then this might be called "hyperscaling" [9].

Hadron charge exchange spectra will face worse energy resolution, sparser statistical accuracy, and larger systematic uncertainties due to the need to detect neutral ejectiles. The spectra will also have strong backgrounds at large energy loss due to the possibility that the reaction has also created isospin one pions, necessarily by an isovector coupling. This work will show the actual data, including any reaction background, but will compare these responses to a simple theoretical expression atop an assumed background, as a standard comparison.

Single-particle responses to hadron beams will be computed using the relativistic formalism which depends upon the

*jerry.peterson@colorado.edu

least momentum held by a bound nucleon, here called ψ, as a fraction of the assumed Fermi momentum k_F for each nucleus. These variables and the responses $\Phi(\psi)$ are computed following the definitions of Ref. [9]. Parameters needed for the transformation from measured doubly differential cross sections to single-particle responses include the binding energy and Fermi momentum, taken from Ref. [16], the Q-value for the difference between the incoming and outgoing charge-changed hadron masses, and the nuclear Coulomb energy for the difference between incoming charged particles and outgoing neutral particles. The number of nucleons struck once-and-only-once $A_{\rm eff}$ is computed in the Glauber model [17], as described in Ref. [18]. The beam-nucleon total cross sections SGT enter these computations, and these are taken as 70% of the free-space beam-nucleon total cross sections, appropriately weighted for neutrons and protons in nuclei, with the lesser value to represent the effects of Pauli blocking [19–23]. Distributions of neutrons and protons are taken to have the same geometrical parameters, derived from measured nuclear charge distributions with the proton charge distribution unfolded [24]. Effective numbers of protons and neutrons for SCX single scattering are then used as $Z_{\rm eff} = Z\,A_{\rm eff}/A$ and $N_{\rm eff} = N\,A_{\rm eff}/A$. More details on the methods are presented in the Appendix of Ref. [9].

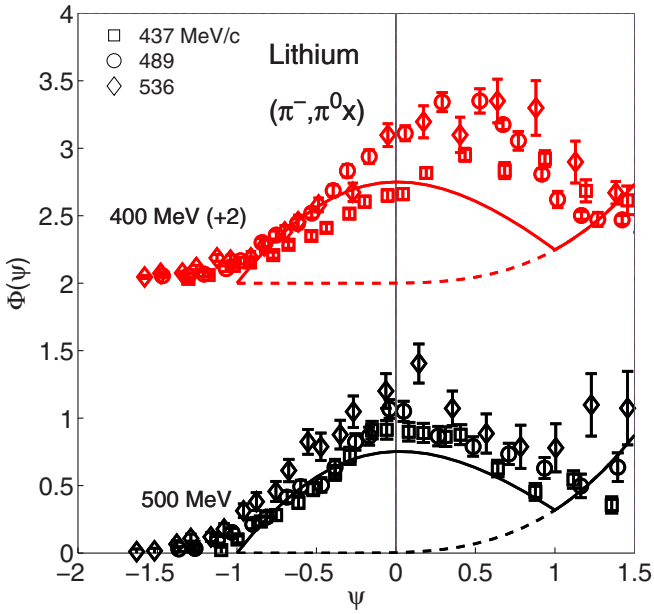

FIG. 1. Inclusive $(\pi^-,\pi^0{\rm x})$ cross-section data [26] for hadron charge exchange on the protons within natural lithium ($A = 7$) have been transformed by the methods of Ref. [9] into relativistic scaling responses at two beam energies for the same momentum transfers, with the 400 MeV data in red in the online figure. The dashed curves show a cubic background, starting at the threshold for pion production (140 MeV) at a momentum transfer of 500 MeV/c, and the solid curves add the relativistic Fermi gas (RFG) expectation without Pauli blocking atop this background. If scaling of the first kind is followed, then the responses for each beam energy and each momentum transfer would be the same for each mass A.

Pion production breaks the condition for "billiard ball" quasifree scattering at large energy losses and is here modeled by a cubic background, as required for p-wave pion production. This cubic background (BG) was also used for SCX responses computed in nonrelativistic y-scaling [25]; here, the form used is $BG(\psi) = BG_0(\psi - \psi_0)^3$, with the factor BG_0 set to match the measured responses $\Phi(\psi)$ at energy losses greater than expected for a quasifree process, and ψ_0 set to match the energy loss threshold to a single nucleon in ψ for pion production (140 MeV) at three-momentum transfer $q = 500\,{\rm MeV}/c$. The Fermi momenta of Ref. [16] are used for the relativistic Fermi gas calculations and in computing ψ and $\Phi(\psi)$.

These Fermi momenta k_F enter into the computation of ψ and of $\Phi(\psi)$ and were obtained from fits to electron scattering data [16]. It is not obvious that these are appropriate to hadrons. A 10% change in k_F leads to about a 10% change in the computed response at $\psi = 0$, and to about a 20% change at $\psi = -0.8$, where interpolated responses are summarized.

II. SCALING OF THE FIRST KIND

Scaling of the first kind has been defined as noting that the responses for a given beam on a given target are independent of the three-momentum transfer q [4,14,15]. Such scaling has been noted for electron longitudinal scattering from nucleon charges [4]. Figures 1–6 show $(\pi^-,\pi^0{\rm x})$ inclusive charge

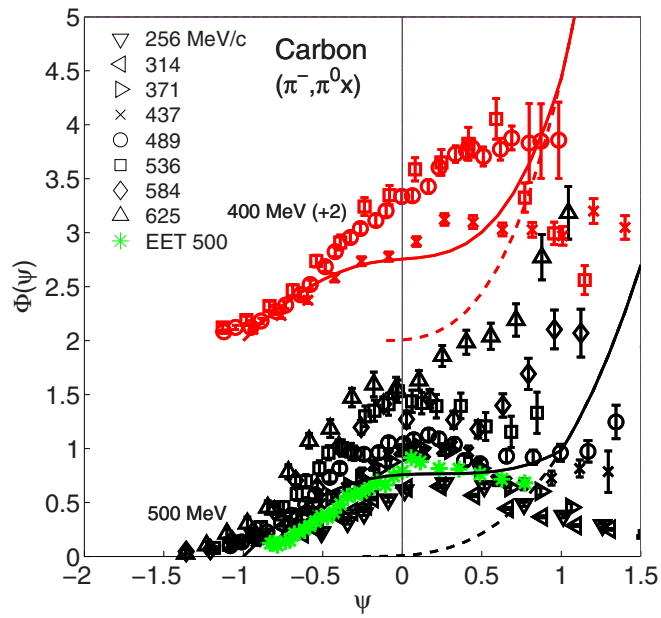

FIG. 2. Inclusive $(\pi^-,\pi^0{\rm x})$ cross-section data [26] for hadron charge exchange on the protons within carbon ($A = 12$) have been transformed by the methods of Ref. [9] into relativistic scaling responses. The dashed curves show a cubic background, starting at the threshold for pion production at a momentum transfer of 500 MeV/c, and the solid curves add the relativistic Fermi gas (RFG) expectation atop this background. Also shown (in green in the online figure) are transverse electron scattering responses (EET) at $q = 500\,{\rm MeV}/c$ [13], using the same methods as for the pion data.

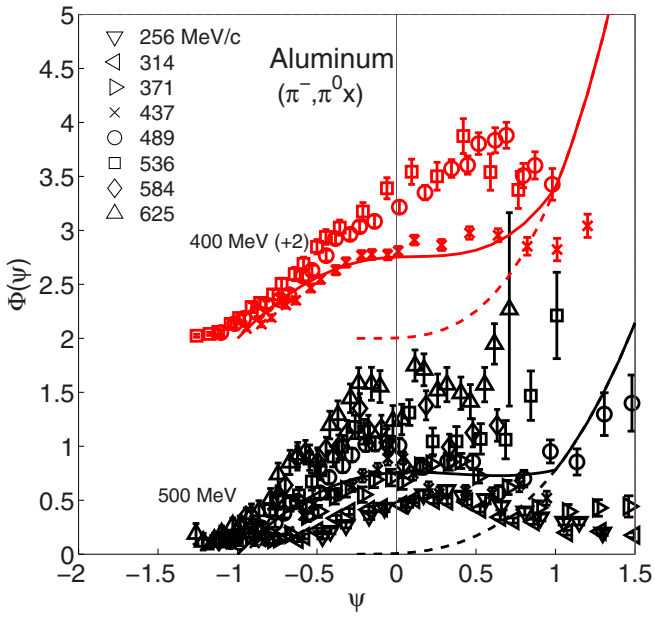

FIG. 3. Inclusive $(\pi^-,\pi^0 x)$ cross-section data [26] for hadron charge exchange on the protons within aluminum ($A = 27$) have been transformed by the methods of Ref. [9] into relativistic scaling responses. The dashed curves show a cubic background, starting at the threshold for pion production at a momentum transfer of 500 MeV/c, and the solid curves add the relativistic Fermi gas (RFG) expectation atop this background.

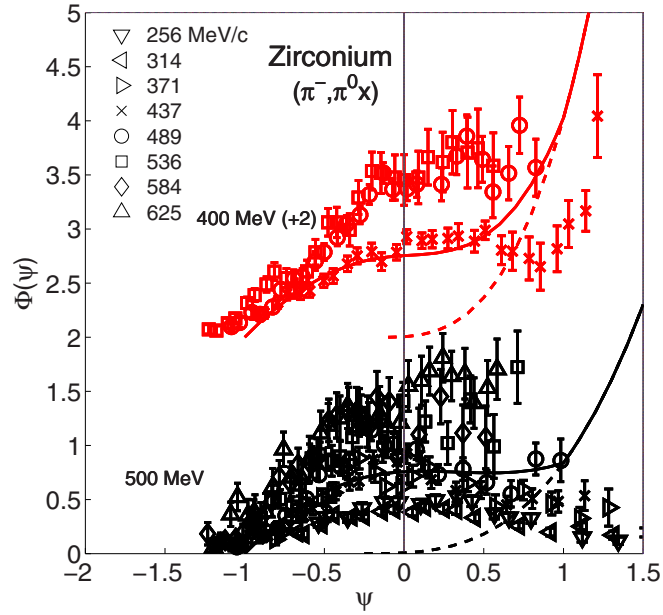

FIG. 5. Inclusive $(\pi^-,\pi^0 x)$ cross-section data [26] for hadron charge exchange on the protons within natural zirconium ($A = 91$) have been transformed by the methods of Ref. [9] into relativistic scaling responses. The dashed curves show a cubic background, starting at the threshold for pion production at a momentum transfer of 500 MeV/c, and the solid curves add the relativistic Fermi gas (RFG) expectation atop this background.

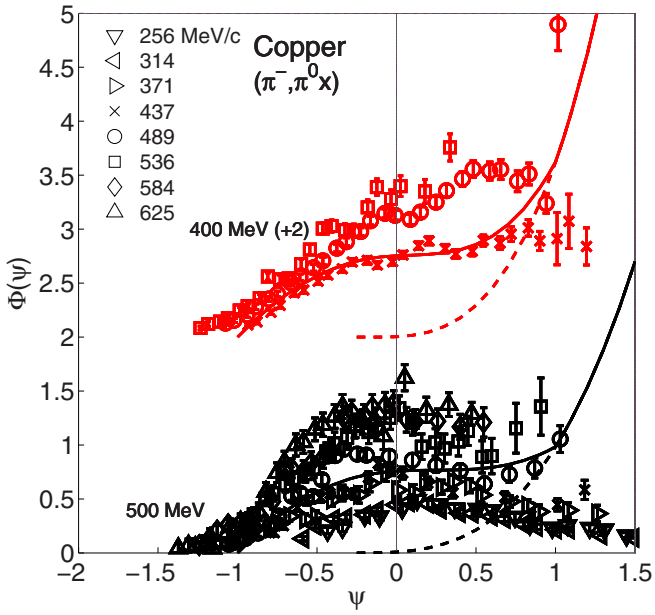

FIG. 4. Inclusive $(\pi^-,\pi^0 x)$ cross-section data [26] for hadron charge exchange on the protons within copper ($A = 64$) have been transformed by the methods of Ref. [9] into relativistic scaling responses. The dashed curves show a cubic background, starting at the threshold for pion production at a momentum transfer q of 500 MeV/c, and the solid curves add the relativistic Fermi gas (RFG) expectation atop this background.

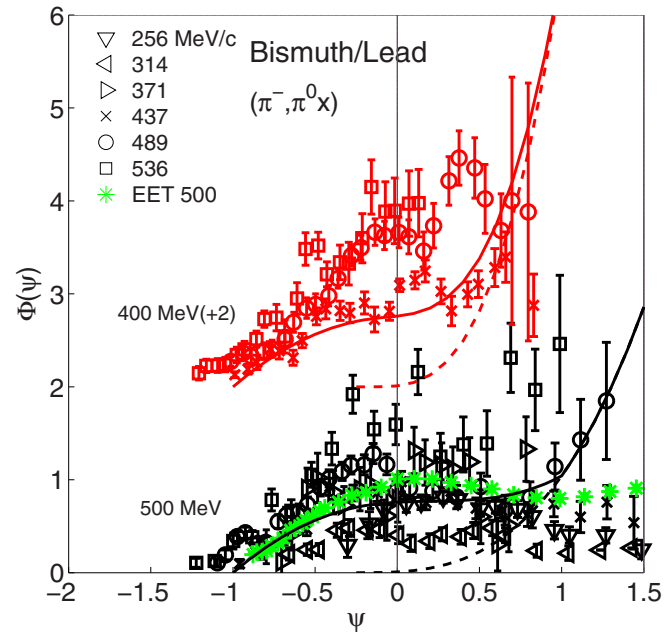

FIG. 6. Inclusive $(\pi^-,\pi^0 x)$ cross-section data [26] for hadron charge exchange on the protons within bismuth ($A = 209$) have been transformed by the methods of Ref. [9] into relativistic scaling responses. The dashed curves show a cubic background, starting at the threshold for pion production at a momentum transfer of 500 MeV/c, and the solid curves add the relativistic Fermi gas (RFG) expectation atop this background. Also shown are transverse electron scattering responses (EET) on lead (in green online) at $q = 500$ MeV/c [13].

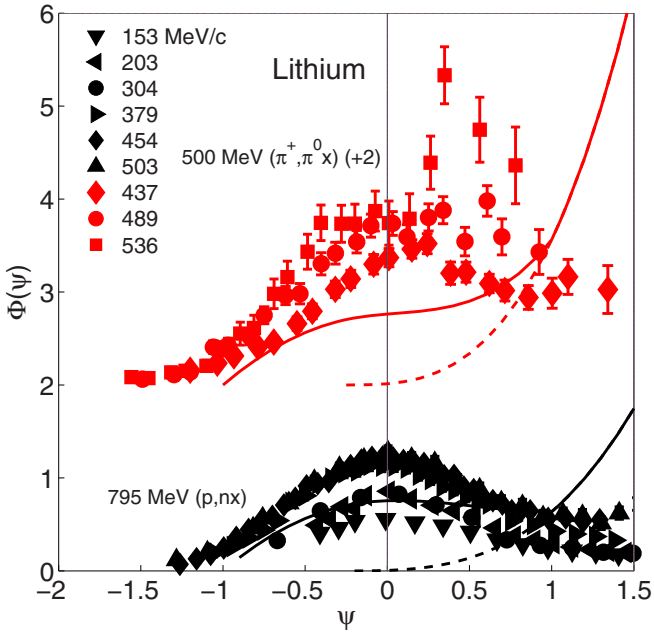

FIG. 7. Inclusive $(\pi^+,\pi^0 x)$ [26] and (p,nx) [27] cross-section data for hadron charge exchange on the neutrons within natural lithium ($A = 7$) have been transformed by the methods of Ref. [9] into relativistic scaling responses. Open data points in the figures of the present work are for negative pions, and solid points are positive beams The dashed curves show a cubic background, starting at the threshold for pion production (140 MeV) at a momentum transfer of 500 MeV/c, and the solid curves add the relativistic Fermi gas (RFG) expectation atop this background. If scaling of the first kind is followed, then the responses for each beam energy and each momentum transfer would be the same for each beam.

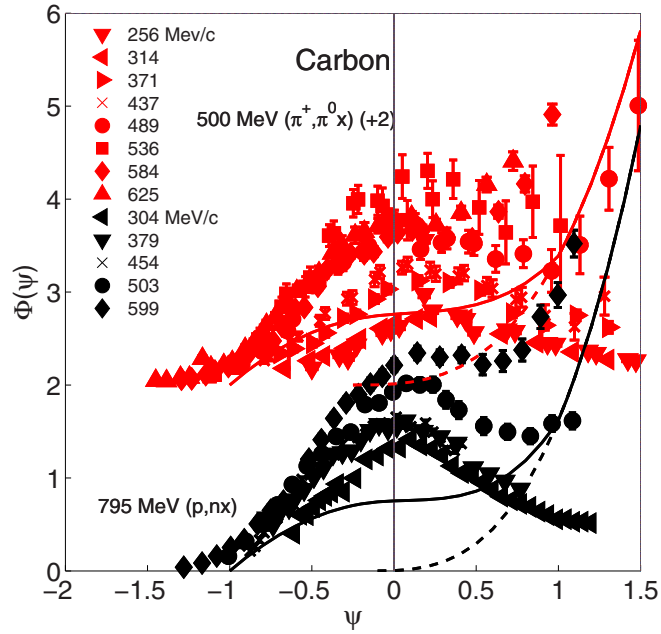

FIG. 8. Inclusive cross sections for 500 MeV $(\pi^+,\pi^0 x)$ [26] and for 795 MeV (p,nx) [27,28] hadron charge exchange on the neutrons within carbon have been transformed by the methods of Ref. [9] into relativistic scaling responses. The dashed curves show a cubic background, starting at the threshold for pion production at a momentum transfer of 500 MeV/c, and the solid curves add the relativistic Fermi gas (RFG) expectation atop this background.

exchange responses from the data of Ref. [26] on bound protons for lithium, carbon, aluminum, copper, zirconium and bismuth at several angles and two beam energies. The curves show an estimated cubic background in ψ and the relativistic Fermi gas (RFG) expectation [4], both at $q = 500\,\mathrm{MeV}/c$, as a consistent comparison. These SCX negative pion data on bound protons do not scale with changing momentum transfer for every mass A, and are above the RFG expectation, even with a strong background, especially for the heavier nuclei.

Charge exchange responses on bound neutrons are compared for 500 MeV $(\pi^+,\pi^0 x)$ [26] and 795 MeV (p,nx) [27,28] on six nuclei in Figures 7–12. It must be noted that the cross sections of Refs. [27,28] differ by a factor of 1.6. The (p,nx) thesis data of Ref. [27] were multiplied by a factor of 1.6 for all cases to match the data of Ref. [28]. The negative pion data were normalized directly to known cross sections for the protons in a CH_2 target, with an estimated systematic uncertainty of about 14% [26]. The positive pion data were normalized so as to force agreement between the pion beam charges for quasifree reactions on deuterium in a CD_2 target, with an estimated uncertainty of 20% [26]. The (p,nx) cross sections of Ref. [28] are stated to have a systematic uncertainty of 9%, and the general average for all the (p, nx) experiments cited in this work is near 10%. Only statistical uncertainties are shown in the present work.

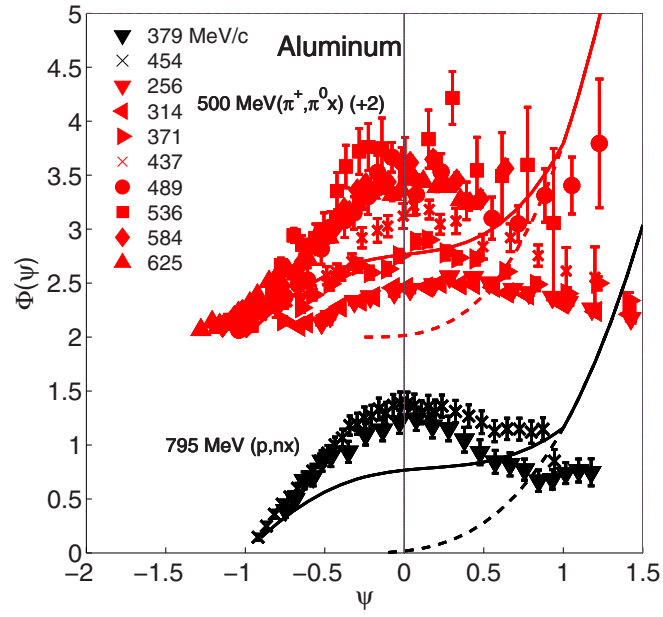

FIG. 9. Inclusive cross sections for 500 MeV $(\pi^+,\pi^0 x)$ [26] and for 795 MeV (p,nx) [27] hadron charge exchange on the neutrons within aluminum have been transformed by the methods of Ref. [9] into relativistic scaling responses. The dashed curves show a cubic background, starting at the threshold for pion production at a momentum transfer of 500 MeV/c, and the solid curves add the relativistic Fermi gas (RFG) expectation atop this background.

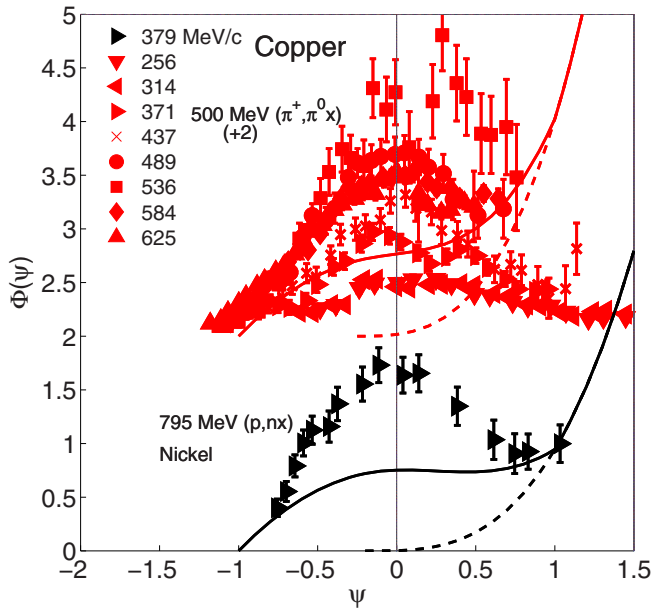

FIG. 10. Inclusive cross sections for 500 MeV $(\pi^+,\pi^0 x)$ on copper [26] and for 795 MeV (p,nx) on nickel [27] hadron charge exchange have been transformed by the methods of Ref. [9] into relativistic scaling responses. The dashed curves show a cubic background, starting at the threshold for pion production at a momentum transfer of 500 MeV/c, and the solid curves add the relativistic Fermi gas (RFG) expectation atop this background.

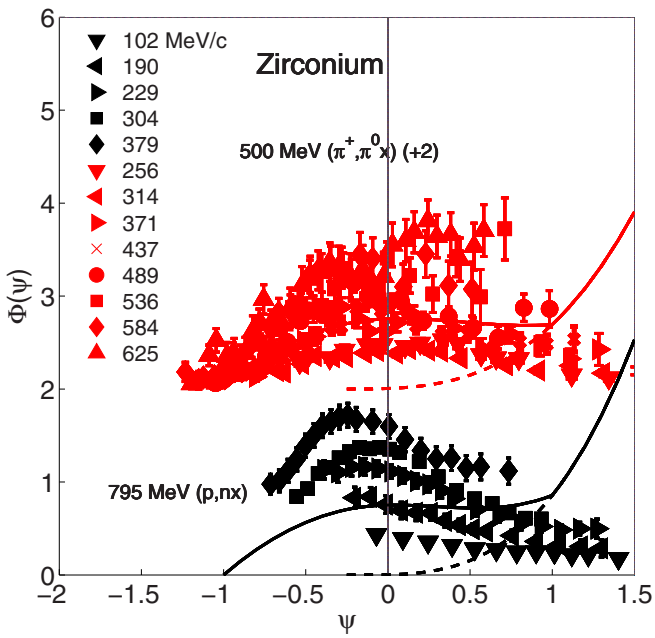

FIG. 11. Inclusive cross sections for 500 MeV $(\pi^+,\pi^0 x)$ [26] and for 795 MeV (p,nx) [27] hadron charge exchange on the neutrons within zirconium have been transformed by the methods of Ref. [9] into relativistic scaling responses. The dashed curves show a cubic background, starting at the threshold for pion production at a momentum transfer of 500 MeV/c, and the solid curves add the relativistic Fermi gas (RFG) expectation atop this background.

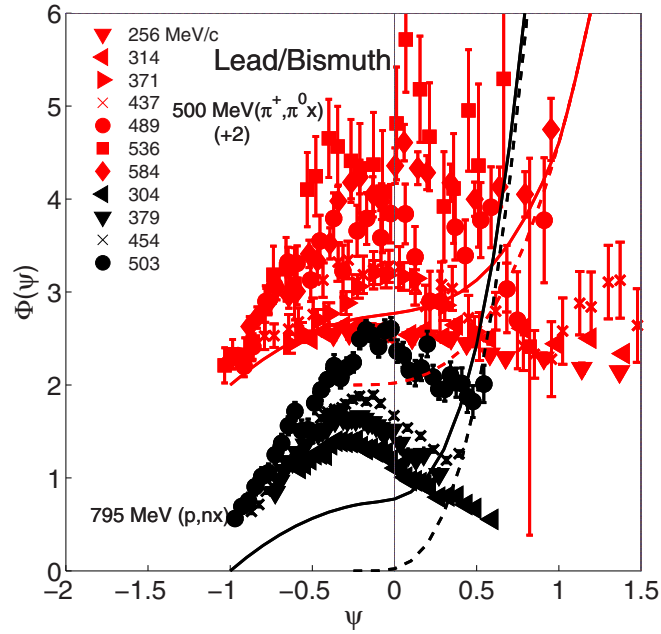

FIG. 12. Inclusive cross sections for 500 MeV $(\pi^+,\pi^0 x)$ [26] and for 795 MeV (p,nx) [27,28] hadron charge exchange on the neutrons within bismuth and lead have been transformed by the methods of Ref. [9] into relativistic scaling responses. The dashed curves show a cubic background, starting at the threshold for pion production at a momentum transfer of 500 MeV/c, and the solid curves add the relativistic Fermi gas (RFG) expectation atop this background.

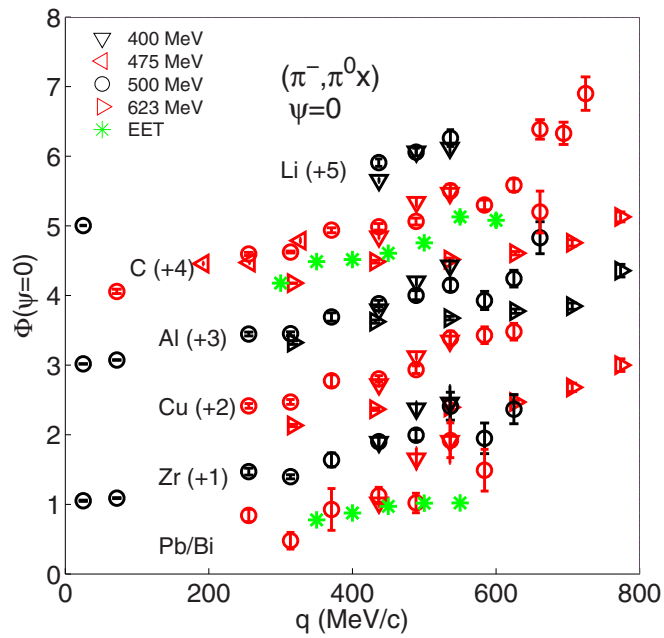

FIG. 13. Interpolated SCX responses on several nuclei $\Phi(\psi = 0)$ for inclusive [26] and exclusive [12] negative pions are shown as the momentum transfer q increases. For carbon and lead samples, these responses are compared to the transverse electron scattering responses derived from the $q = 500$ MeV/c data of Ref. [13]. The exclusive 623 MeV pion experiment included one-and-only-one neutral pion [12].

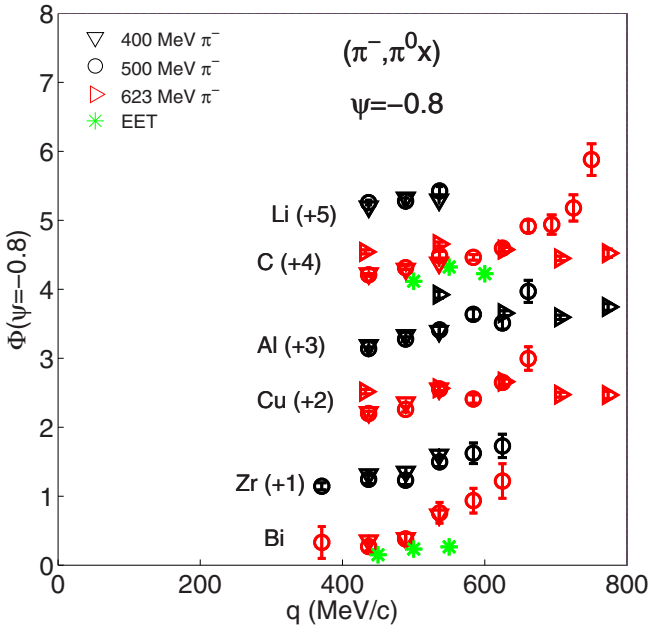

FIG. 14. As for Fig. 13, but interpolated responses are shown at $\psi = -0.8$, further from background reaction processes.

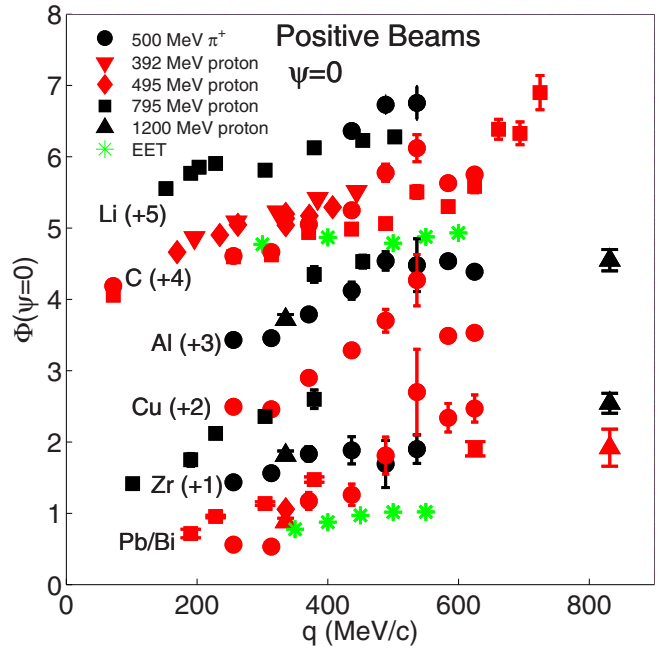

FIG. 15. Interpolated SCX responses $\Phi(\psi = 0)$ on several nuclei for inclusive positive pions [26] and several proton beam energies [27–29,33–36] are shown as the momentum transfer q increases. Transverse electron data [13] at $q = 500\,\mathrm{MeV}/c$ are in green in the online figures.

Scaling of the first kind is noted for lithium over some range of momentum transfers, but this is lost for heavier nuclei, and the responses for heavier nuclei are far above the RFG expectation with the cubic background. The two positive hadron beams do, however, find similar SCX responses on bound neutrons for similar momentum transfers, stronger than for the SCX responses on bound protons as noted for negative pions.

These six sets of SCX responses for negative pion and transverse electron [13] beams are summarized in Figs. 13 and 14, where responses $\Phi(\psi)$ interpolated at $\psi = 0$ and -0.8 are plotted as the momentum transfer q increases. These hadronic responses all increase with q, not scaling as expected for the first kind. The exclusive data at 623 MeV (750 MeV/c) [12] lie below the inclusive data and rise less rapidly as q increases. For carbon the exclusive negative pion data at 623 MeV are nearly consistent with the transverse electron scattering responses for carbon.

Similar interpolated SCX responses for positive beams are shown in Figs. 15 and 16. The responses at $\psi = 0$ are more scattered, and not consistent as the proton beam energy is changed. Further from the pion production, responses at $\psi = -0.8$ are much more consistent and are stronger than the transverse electron interpolation for carbon.

III. SCALING OF THE SECOND KIND

If the responses derived from measured cross sections for a given beam and a fixed momentum transfer are the same for a wide range of nuclei, then this effect has been called scaling of the second kind [4,14,15]. This is tested for SCX at q near 500 MeV/c as shown in Fig. 17 for both pion signs and two pion beam energies. These data have not been adjusted for possible backgrounds. For nuclei of masses $A = 7$ through $A = 209$, these responses for each beam are quite similar, with the positive pion responses notably stronger than for negative pions. At lower momentum transfers for $A = 7$

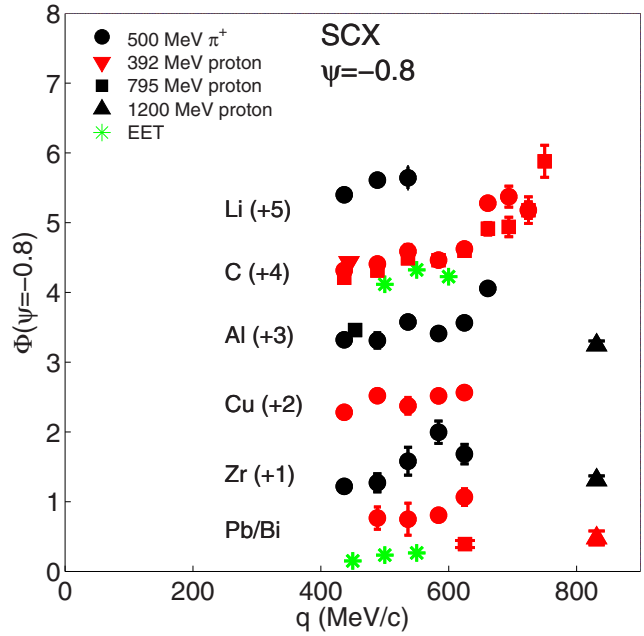

FIG. 16. As Fig. 15, but for interpolated SCX responses at $\psi = -0.8$, including transverse electron data [13].

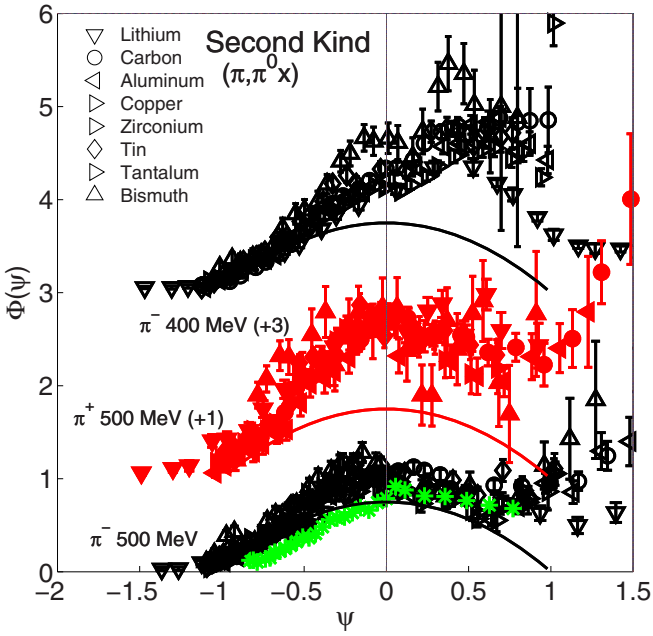

FIG. 17. To demonstrate scaling of the second kind, SCX response data are shown for both pion signs [26] for momentum transfers $q = 489\,\mathrm{MeV}/c$. Solid points are for positive beams and open points are for negative pion beams. Green symbols are for transverse electron scattering on carbon at $q = 500\,\mathrm{MeV}/c$ [13]. The solid curve shows the relativistic Fermi gas expectation for $q = 500\,\mathrm{MeV}/c$ with $k_\mathrm{F} = 238\,\mathrm{MeV}/c$.

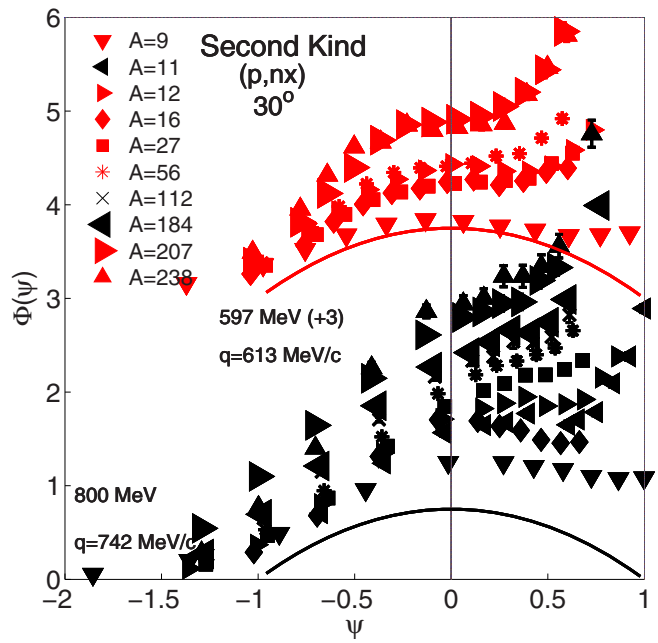

FIG. 18. Responses computed from the extensive (*p,nx*) data set for 800 MeV [30] and 597 MeV [31] at 30 degrees ($q = 742$ and 613 MeV/c) are shown for a wide range of nuclear masses A to test scaling of the second kind. For comparison, the RFG curves are shown.

through $A = 238$, the 795 MeV proton SCX experiment [27] finds near agreement with scaling of the second kind, as shown in Fig. 18. For larger momentum transfers, this 795 MeV proton experiment and the similar SCX study at a proton energy of 800 MeV [29] yield relativistic responses $\Phi(\psi)$ that increase strongly with increasing nuclear mass A, seemingly due to strong backgrounds for pion production, as seen in previous figures.

At larger momentum transfers, the short flight path (*p,nx*) data of Refs. [30,31], which covered a wide range of nuclei, are shown in Fig. 18. Scaling of the second kind is not observed at these large momentum transfers, with responses increasing strongly with target mass, and no similarity to the RFG expectation for nuclei beyond beryllium.

Figure 19 shows SCX responses from the 1200 MeV (*p,nx*) data [29]. Good scaling of the second kind is observed, although the 25 degree data do not match the RFG curve shown.

These SCX results and others are summarized in Figs. 20 and 21, which show interpolated values of the measured responses for three pion beams at $\psi = 0$ (the expected maximum) and at $\psi = -0.8$ (where background effects will be smaller). Solid data points are for positive beams, open points are for negative pions, all for q near $500\,\mathrm{MeV}/c$. At the higher proton energy of 1200 MeV at two angles, the responses derived from the cross sections of Ref. [29] at both $\psi = 0$ and $\psi = -0.8$ are remarkably consistent as the nuclear mass A increases, as shown in Figs. 20 and 21. There is little change for each beam with the changing mass of the nucleus, demonstrating good scaling of the second kind for hadron SCX, but the interpolated responses do change with beam species and beam energy.

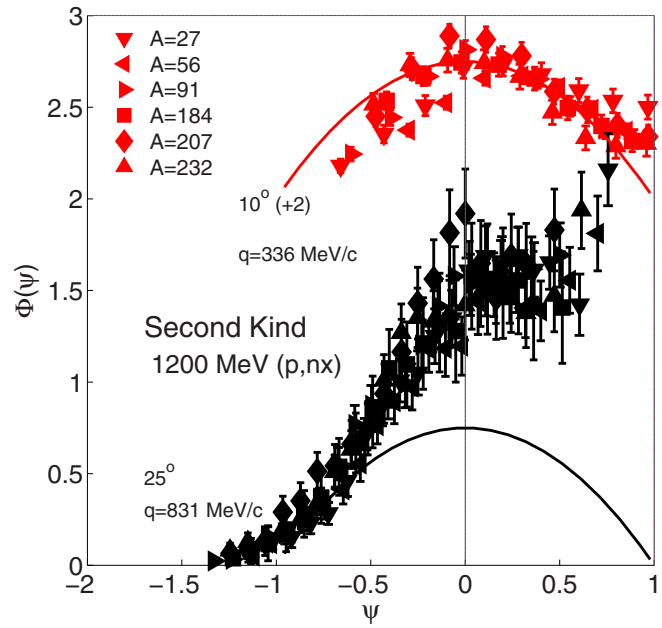

FIG. 19. Responses to 1200 MeV proton SCX [29] at two angles ($q = 336$ and 831 MeV/c) are shown for a range of nuclear masses A.

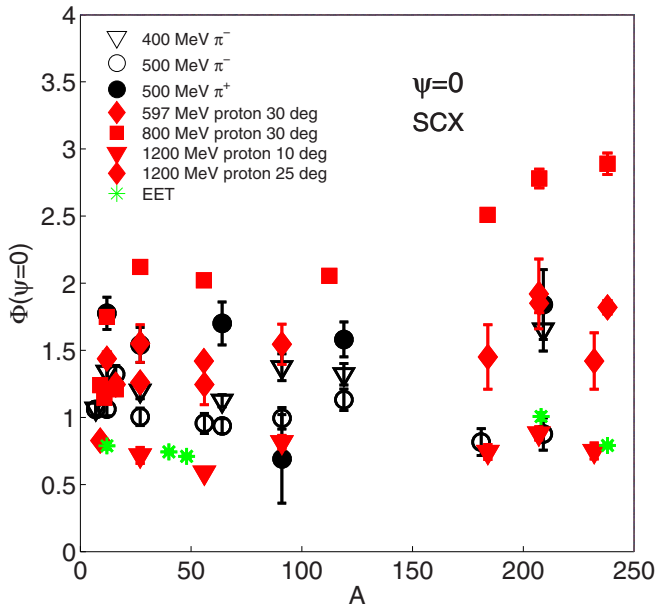

FIG. 20. Interpolated responses $\Phi(\psi = 0)$ are shown for both signs of pion SCX [26] at $q = 489\,\mathrm{MeV}/c$, for the 30 degree (p,nx) data [30,31], and for the 10 and 25 degree data at 1200 MeV [29] for a range of target masses A. Solid points are for positive beams and open points are for negative pions. Relativistic responses at $q = 500\,\mathrm{MeV}/c$ for transverse electron scattering (EET) are shown online as green stars [13].

Much as noted for the responses to electron scattering [13] and for NCX hadron scattering [9], hadron SCX responses demonstrate good scaling of the second kind, with the only free parameter being the 70% of free-space total cross sections

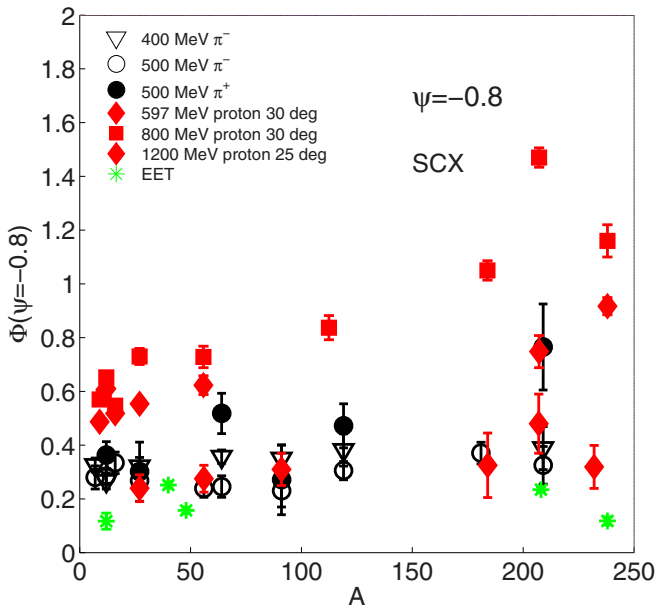

FIG. 21. Same as described in the caption of Fig. 20, but for responses interpolated at $\psi = -0.8$.

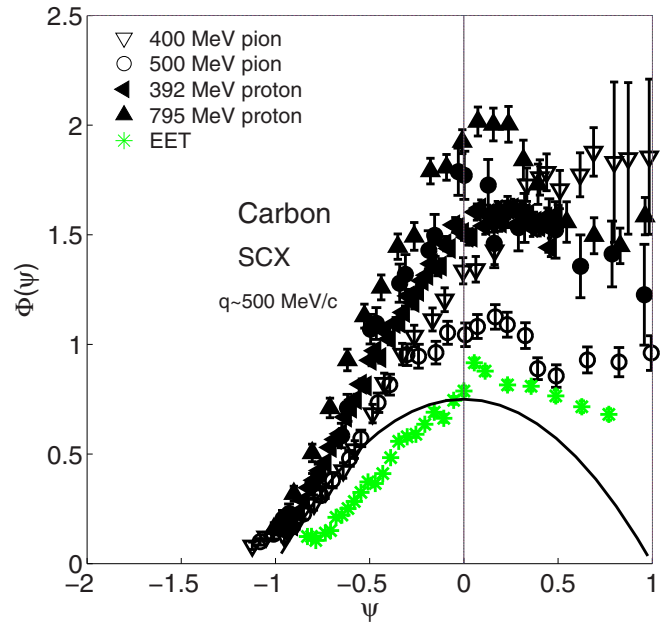

FIG. 22. If responses to all beams were the same for a given target mass A and momentum transfer q, then this would be scaling of the third kind. SCX response data are shown for carbon ($A = 12$) for a momentum transfer q near 500 MeV/c, with data from Refs. [13,26–28,33]. Solid points are for positive beams and open points are for negative pions.

used in the Glauber computation of the effective number of nucleons.

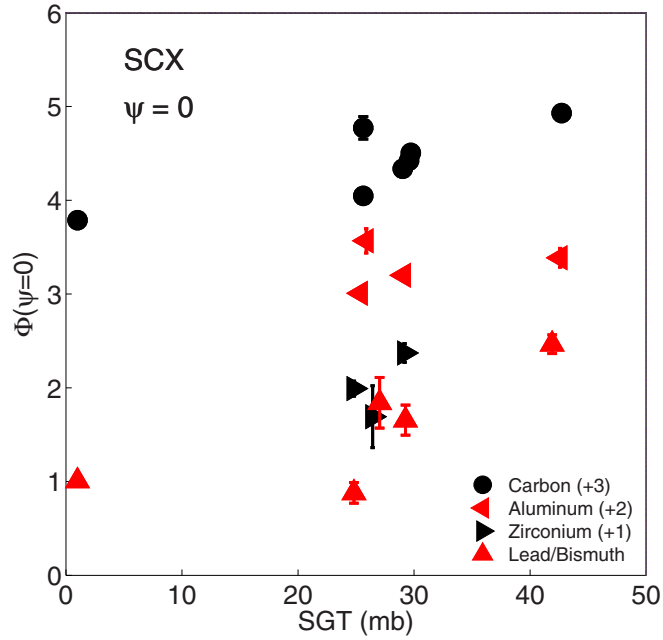

FIG. 23. Scaling of the third kind is demonstrated by displaying interpolated SCX responses $\Phi(\psi = 0)$ for several nuclei for a number of beams [13,26–29,32,36] versus their free-space beam-nucleon total cross sections SGT [37]. Only cases with q near 500 MeV/c are included.

IV. SCALING OF THE THIRD KIND

Scaling of the third kind would hold if all incident beams upon a given nucleus at similar momentum transfers were to have the same responses, within mutual systematic uncertainties of about 26% for all SCX experiments. Figure 22 shows relativistic $\Phi(\psi)$ responses from hadron SCX data on carbon at momentum transfers q near 500 MeV/c for 500 MeV pions (of both charge states) and proton SCX at several beam energies. A distinct maximum in these responses is noted at $q = 350\,\mathrm{MeV}/c$, but the magnitudes of the responses are not the same, with lower beam energy protons giving stronger SCX responses. Stronger responses are seen for q near 500 MeV/c, and these are again not equal in magnitude.

The beam species differ in their total cross sections (SGT) on the average of neutrons and protons within a complex nucleus. Figure 23 plots the interpolated SCX responses for both pion and proton beams at $\psi = 0$ for several nuclei as this free-space total cross section increases [37], including transverse (mostly isovector) electron scattering [13]. Only 70% of the free-space total cross sections were used to compute A_{eff} as used in the computations for the responses Φ. The momentum transfer is near $q = 500\,\mathrm{MeV}/c$ for these data. The sparse data rise only slowly with increasing total beam-nucleon cross sections, except for the heaviest sample.

Farther from background reactions, Figure 24 shows interpolated responses at $\psi = -0.8$, with remarkably flat slopes as the total cross section increases, demonstrating good scaling of the third kind.

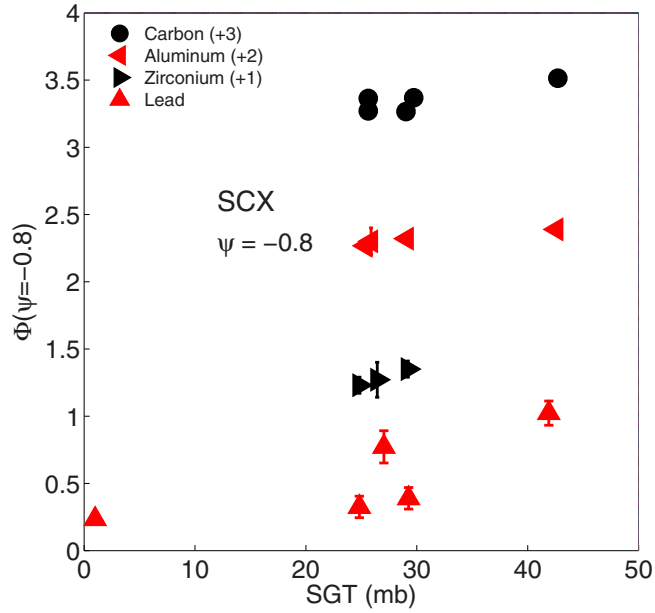

FIG. 24. Same as described in the caption of Fig. 23, but for SCX responses interpolated at $\psi = -0.8$.

V. CONCLUSIONS

Scaling of the first kind for hadronic SCX has been tested with a very wide range of relativistic responses for hadron charge exchange quasifree cross sections. This scaling is violated, more so for heavier nuclei and at three momentum transfers q above 600 MeV/c, and more so at larger energy losses. Figures 13–16 provide interpolated examples for charge exchange on bound protons and on bound neutrons as the momentum transfer changes. These trends with q are also noted in (mostly) isovector transverse responses for electron scattering.

Scaling of the second kind at nearly the same momentum transfer, in contrast, is closely followed, as shown in Figs. 20 and 21, except for large momentum transfers, as seen in Fig. 18. The responses $\Phi(\psi)$ for different beam species do not agree, however.

Scaling of the third kind for a range of beam species and beam energies is not observed in Figs. 20 and 21, but is seen to be related to the beam-nucleon total cross section in Figs. 23 and 24. For four sample nuclei these responses rise slowly with the free space total cross sections SGT [37] at large energy losses ($\psi = 0$), but are nearly constant at $\psi = -0.8$, farther from pion production and other complications.

The observation that hadron charge exchange responses on bound neutrons are larger than for SCX on bound protons, and the fact that hadron beams are scattered simply mainly by nucleons in the nuclear surface, leads one to suspect that the assumed geometrical symmetry between neutron and proton distributions in the nucleus is not valid. The above calculations use the Glauber method to compute Z_{eff} and N_{eff}, using the same distributions for bound protons and bound neutrons, measured by electron scattering from nuclear charge [24]. A future paper will explore the option of differing neutron and proton distributions within nuclei, including the effects upon total and total reaction cross sections for hadrons on complex nuclei.

[1] M. L. Goldberger and K. M. Watson, *Collision Theory* (John Wiley, New York, 1964).
[2] D. B. Day, J. S. McCarthy, T. W. Donnelly, and I. Sick, Annu. Rev. Nucl. Part. Sci. **40**, 357 (1990).
[3] O. Benhar, D. Day, and I. Sick, Rev. Mod. Phys. **80**, 189 (2008).
[4] T. W. Donnelly and I. Sick, Phys. Rev. C **60**, 065502 (1999).
[5] A. N. Antonov, M. K. Gaidarov, D. N. Kadrev, M. V. Ivanov, E. M. de Guerra, and J. M. Udias, Phys. Rev. C **69**, 044321 (2004).
[6] J. E. Amaro, M. B. Barbaro, J. A. Caballero, T. W. Donnelly, A. Molinari, and I. Sick, Phys. Rev. C **71**, 015501 (2005).
[7] A. N. Antonov, M. K. Gaidarov, M. V. Ivanov, D. N. Kadrev, E. Moya de Guerra, P. Sarriguren, and J. M. Udias, Phys. Rev. C **71**, 014317 (2005).
[8] Joanna E. Sobczyk, Phys. Rev. C **96**, 045501 (2017).
[9] R. J. Peterson, Phys. Rev. C **98**, 024606 (2018).
[10] J. A. Caballero, J. E. Amaro, M. B. Barbaro, T. W. Donnelly, and J. M. Udias, Phys. Lett. B **653**, 366 (2007).

[11] E. S. Pinzon Guerra *et al.*, Phys. Rev. D **99**, 052007 (2019).
[12] R. J. Peterson *et al.*, Phy. Rev. C **69**, 064612 (2004).
[13] A. Zgiche *et al.*, Nucl. Phys. A **572**, 513 (1994).
[14] A. N. Antonov, M. V. Ivanov, J. A. Caballero, M. B. Barbaro, J. M. Udias, E. Moya de Guerra, and T. W. Donnelly, Phys. Rev. C **83**, 045504 (2011).
[15] R. Gonzalez-Jimenez, G. D. Megias, M. B. Barbaro, J. A. Caballero, and T. W. Donnelly, Phys. Rev. C **90**, 035501 (2014).
[16] C. Maieron, T. W. Donnelly, and I. Sick, Phys. Rev. C **65**, 025502 (2002).
[17] R. J. Glauber, in *Lectures in Theoretical Physics*, Vol. 1, edited by W. J. Brittin and L. G. Dunham (Wiley, New York, 1959), p. 315.
[18] J. Ouyang, S. Høibråten, and R. J. Peterson, Phys. Rev. C **47**, 2809 (1993).
[19] R. D. Smith and M. Bozoian, Phys. Rev. C **39**, 1751 (1989).
[20] L. Ray, Phys. Rev. C **41**, 2816 (1990).
[21] J. J. Kelly, Phys. Rev. C **54**, 2547 (1996).
[22] C. Fuchs, A. Faessler, and M. El-Shabshiry, Phys. Rev. C **64**, 024003 (2001).
[23] I. C. Cloet, W. Bentz, and A. W. Thomas, Phys. Rev. Lett. **116**, 032701 (2016).
[24] J. D. Patterson and R. J. Peterson, Nucl. Phys. A **717**, 235 (2003).
[25] R. J. Peterson, Nucl. Phys. A **769**, 115 (2006).
[26] J. Ouyang, Ph.D. thesis, University of Colorado, 1992; Los Alamos report LA-12457-T (1992).
[27] D. L. Prout, Ph.D. thesis, University of Colorado, 1992.
[28] D. L. Prout *et al.*, Phys. Rev. C **52**, 228 (1995).
[29] S. Leray *et al.*, Phys. Rev. C **65**, 044621 (2002).
[30] W. B. Amian *et al.*, Nucl. Sci. Eng. **112**, 78 (1992).
[31] W. B. Amian *et al.*, Nucl. Sci. Eng. **115**, 1 (1993).
[32] T. Wakasa *et al.*, Phys. Rev. C **59**, 3177 (1999).
[33] H. Otsu, Ph.D. thesis, University of Tokyo, 1995.
[34] X. Y. Chen *et al.*, Phys. Rev. C **47**, 2159 (1993).
[35] J. B. McClelland *et al.*, Phys. Rev. Lett. **69**, 582 (1992).
[36] B. A. Luther, Ph.D. thesis, The Ohio State University, 1993.
[37] http//gwdac.physics.gwu.edu.